Optical and Quantum Electronics (2024) 56:1804
https://doi.org/10.1007/s11082-024-07713-9

An investigation on optical, dielectric and thermal analysis of semiorganic bisglycine cobalt chloride dihydrate single crystal for electronic and opto-electronic devices

P. Revathi[1] · T. Balakrishnan[2] · J. Thirupathy[3]

Received: 19 March 2024 / Accepted: 8 October 2024

Abstract
Semiorganic single crystal of bisglycine cobalt chloride dihydrate (BGCCD) is a superior material for non-linear optics (NLO) applications such as photonic, electronic and opto-electronic devices. This article presents high-quality BGCCD single crystals prepared using the slow evaporation solution technique (SEST), which are a famous NLO material. A transparent BGCCD crystal with a maximum size of $9\times9\times8$ mm^3 was collected over the period of 80 days. Various analyses were conducted on the grown crystals, including single crystal x-ray diffraction, which was utilized to find out the unit cell parameters. Analyses of functional groups using Fourier transform infrared spectroscopy. Finding the band gap and absorbance of the grown crystal is done using UV-Visible spectroscopy. Mechanical stability is determined by micro-hardness. The dielectric loss and dielectric constant of the grown crystal is found by utilizing dielectric measurements. The stability is found through thermo-gravimetric and differential thermal analyses. To detect surface flaws in the grown crystals, etching analysis was employed. Structure morphology was identified using a scanning electron microscope. The elements were identified using energy dispersive x-ray analysis. The excitation and emission spectra can be determined using photoluminescence, and in order to determine the crystal's thermal diffusivity, photoacoustic spectroscopy was employed. The findings regarding thermal diffusivity indicate that it is well-suited for uses related to opto-electronic devices.

Keywords Crystal growth · Optical analysis · Dielectric analysis · Thermal analysis

✉ P. Revathi
revathidhanam777@gmail.com

✉ J. Thirupathy
thirupathyj1@gmail.com

[1] Department of Physics, Jamal Mohamed College (Autonomous), Trichy 620 020, Tamilnadu, India

[2] PG and Research Department of Physics, Thanthai Periyar Government Arts and Science College (Autonomous), Trichy 620 023, Tamilnadu, India

[3] Department of Physics, Marudhar Kesari Jain College for Women, Vaniyambadi 635 751, Tamilnadu, India

Published online: 26 October 2024

1 Introduction

Nowadays many researchers interested to grow semiorganic nonlinear optical (NLO) materials because of the large flexibility in molecular design, higher NLO efficiency and application in the extension of the limited and fixed frequency outputs available from lasers (Chemla and Zyss 1987). High NLO coefficients and outstanding mechanical and thermal properties are exhibited by semiorganic NLO crystals (Venkataramanan et al. 1995). A lot of study has focused on the possible photonic applications of amino acids and their complexes in this area (Marder et al. 1991). L-Arginine and L-Arginine phosphate are second harmonic generators that work well in devices like optical parametric amplifiers (Eimerl et al. 1989). For infrared detectors and the room-temperature target component of vidicon, tricrylium sulphate has proven a crucial substance (Matthias et al. 1956). Anion, cation, or zwitterion forms of the simplest amino acid, glycine (H_2N - CH_2 - COOH), can be found in the molecules (Fleck and Bohaty 2004). An alternative class of amino acids is optically inert and lacks an asymmetric carbon atom (Neurath 1972; Bagavan and Biochemistry 2002). A number of compounds had their structures thoroughly examined; these include halogenides and metal halogenides combined with glycine (Michel Fleck 2008). Alkali metals (Balakrishnan and Ramamurthi 2006; Balu et al. 2009; Sankar et al. 2007; Khandpekar and Pati 2011; Ra. Shanmugavadivu et al. 2006; Lenin et al. 2009), alkaline earth metals (SenthilPandian and Ramasamy 2008; Thomas Joseph Prakash et al. 2008; Dhanaraj and Rajesh 2011), transition metals (Balakrishnan and Ramamurthi 2008; Versiane et al. 2006; Raju et al. 2012), and halogens (NarayanaMoolya and Dharmaprakash 2006, 2007; Selvaraju et al. 2006; Pepinsky et al. 1958; Narayanan and Venkataraman 1975) are among the metals with which glycine complexes have been synthesized for the purpose of learning their structural, mechanical, thermal, and optical properties. An examination of the literature reveals the existence of two research publications concerning materials based on bis-glycine [27–28]. Crystals of bisglycine cobalt chloride dihydrate (BGCCD) are generated using the slow evaporation solution method (SEST) in this article. Several characterization techniques were employed on the grown crystals, including micro-hardness, dielectric, thermo-gravimetric, differential thermal, etching, scanning electron microscopy, energy dispersive x-ray, photoluminescence, photoacoustic spectroscopy, and Fourier transform infrared spectroscopy. Photonic, electrical, and opto-electronic device applications are proposed for the BGCCD crystal based on the characterization results.

2 Experimental section

2.1 BGCCD crystal growth by SEST method

An equimolar combination of glycine and cobalt chloride hexahydrate in double distilled water was used as a ligand to produce BGCCD single crystals. By dissolving the appropriate amount of BGCCD salt in double-distilled water, a solution was formed. The solution was heated and then left to evaporate until it got to room temperature. A series of recrystallizations was used to improve the synthesised salt's purity. Using whatman No. 1 filter paper, a 50 ml saturated solution was filtered. The aluminium foil was used to seal the filter solution,

allowing for regulated evaporation. Figure 1 shows the developed crystal after 85 days of harvesting the high-quality BGCCD single crystal.

3 Results and discussion

3.1 Single crystal X-ray diffraction

The unit cell parameters of the grown BGCCD crystal are obtained using single crystal X-ray diffraction with Bruker platform diffractometer (Mo, Kα = 0.71073Å). It is observed that the BGCCD crystal belongs to monoclinic system with the cell parameters of a = 10.462, b = 5.766, c = 8.58, α = 90°, β = 91.57 and γ = 90°. The calculated cell volume is 560.54 A^3. The cell parameter of BGCCD crystal is a good agreement among the reported values (Fleck and Bohaty 2004).

3.2 FT–IR and FT–Raman spectral analysis

It is via vibrational spectroscopy that crystalline environments, molecular distortions, isomerism, forces between and within molecules, vibrational interactions, and molecular structure may be understood. A Perkin Elmer FT-IR spectrometer was utilised to collect the KBr pellet technique FT-IR and FT-Raman spectra. The FT-IR spectrum in the 400–4000 cm^{-1} wavelength range was recorded using a BRUKER RFS 27 FT-Raman spectrometer, whereas the FT-Raman spectrum in the 50–4000 cm^{-1} wavelength range was recorded

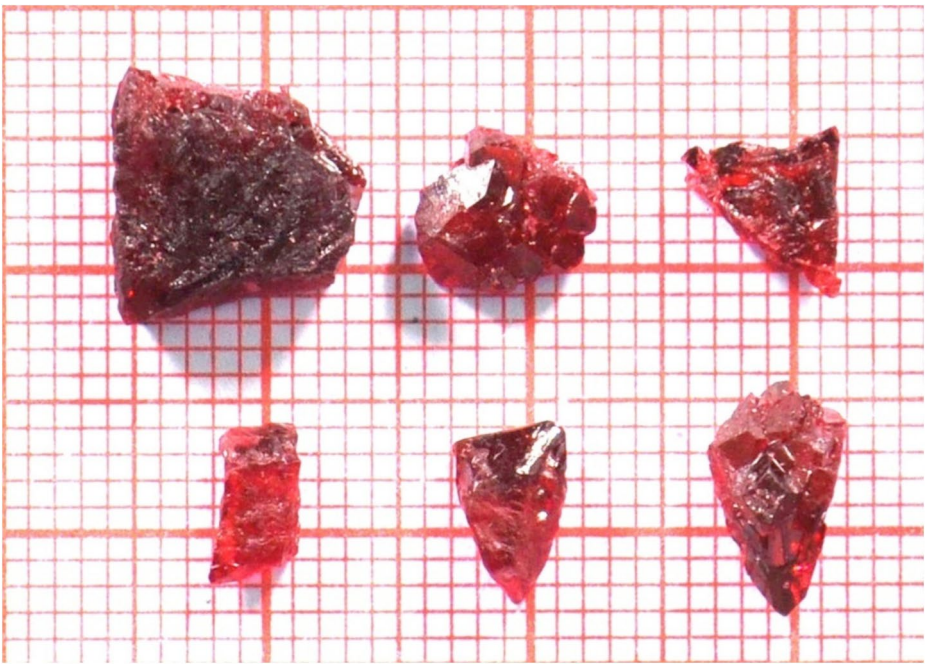

Fig. 1 Photograph of as grown BGCCD single crystal

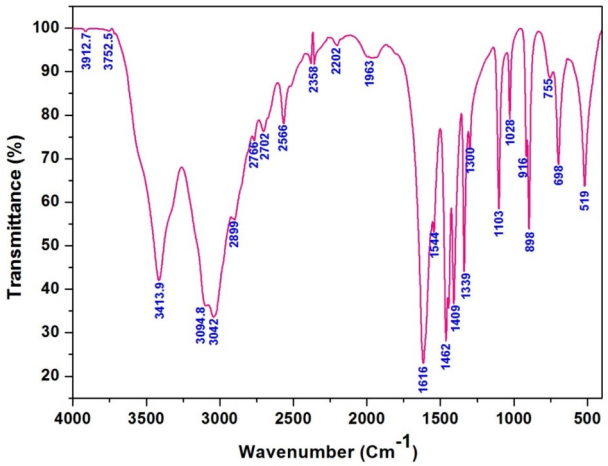

Fig. 2 FT–IR spectrum of BGCCD single crystal

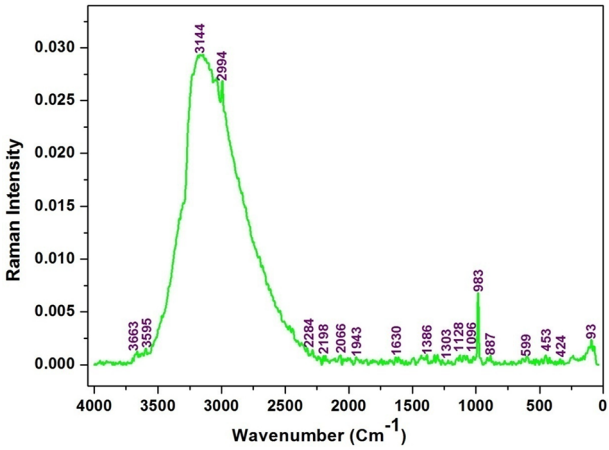

Fig. 3 FT–Raman spectrum of BGCCD single crystal

using a separate instrument. Figure 2 displays the FT-Raman spectra, whereas Fig. 3 displays the BGCCD FTIR spectra. Vibrations of the NH_3^+, CH, CH_2, and COO-functional groups within crystalline glycine cobalt chloride may be caused by molecular influences. The wide band in the high wave number area indicates the existence of hydrogen bonding. Amino acid NH_3+ion presence is indicated by absorption in the 3400–2100 cm^{-1} range. N-H and O-H bonds are the most common types of hydrogen bonds. In a BGCCD crystal, the glycine molecule has a proton on the amino (NH_3+) and deproton on the carboxylate (COO-) groups. The protonation of the amino group may be confirmed by the existence of a prominent band at 1616 cm^{-1}, which corresponds to the asymmetric deformation of NH_3^+. The NH_3^+ ion in BGCCD exhibited asymmetric stretching vibration at wavenumbers of 3094 and 3144 cm^{-1}. The band is displaced in the Brillouin zone centre direction at a wavenumber of 3042 cm^{-1} in the body-centered cubic lattice. Moreover, the occurrence of absorption bands at 2566, 2380, 2358, 2202, 2284, 2198, 2066, and 1943 cm^{-1} can be ascribed to the overlapping of NH^{3+} bending and C-H stretching vibrations, specifically their overtone and combination bands. The presence of carboxylic acid groups (COOH) is

revealed by a distinct absorption band at 1336 cm^{-1}, which corresponds to the stretching of the C=O bond in the COOH group (Gobinathan and Boopathy 2016; Nakamoto 1978). The bands that were detected, together with their corresponding vibrational assignment, are summarised in Table 1.

3.3 Optical studies

The UV-VIS-NIR spectra were recorded using a Thermo Fisher Scientific spectrophotometer and a ranging from 190 to 1100 nm was used in the study. A scanning speed of 750 mm/min was used for this. In Fig. 4 shows that the UV absorbance spectra of the BGCCD crystal, which have a UV lower cutoff wavelength of 288 nm. The optical absorption coefficient (a) is computed from the $\alpha(\nu) = \frac{1}{t}\log\left(\frac{1}{T}\right)$ relation (Socrates 2001). Where, T is the transmittance and t is the thickness of the grown crystal. The crystal band gap can be obtained from the absorption coefficient (a) using the relation (Mott and Davis 1979; Davis and Mott 1970) $\alpha(\nu) = \frac{A(h\nu - E_{opt})^n}{h(\nu)}$ where E_g is the optical band gap energy of the crystal, h is the Planck's constant, υ is the frequency and A is a constant. By expanding upon the linear section in Fig. 5, close to the beginning of the absorption edge, the relationship between the change in $(\alpha h\upsilon)^2$ and h, y and the band gap was calculated. Band gap energy of 5.55 eV has been measured for BGCCD.

Table 1 Vibrational assignment of BGCCD single crystal

FT – IR	FT – Raman	Band assignments
3912	-	NH_3^+ symmetric stretching vibration
3752	-	NH_3^+ asymmetric stretching vibration
-	3663	O – H stretching
3413	3595	O-H asymmetric stretching
3094	3144	NH_3+asymmetric stretching vibration
2899	2994	NH asymmetric stretching vibration
2766	-	NH asymmetric stretching vibration
2702	-	CH stretching
-	1630	CH_2 stretching
1616	-	COO^-asymmetric stretching
1544	-	COO−symmetric stretching
1462	-	CH_2 deformation scissoring
1444	-	CH_2 scissoring vibration
1409	1386	CH_2 wagging
1339	1327	C=O symmetric stretching vibration
1300	1303	NH_3^+rocking vibration
1103	1128	NH_3^+rocking vibration
1028	1096	CCN asymmetric stretching vibration
916	983	CH_2 rocking vibration
897	887	C – C symmetric stretching
755	-	COO^- wagging vibration
698	-	COO^- scissoring
519	599	COO^-rocking vibration
-	453	Co – Cl stretching vibration
-	424	Co – Cl stretching vibration
-	93	Co – Cl stretching vibration

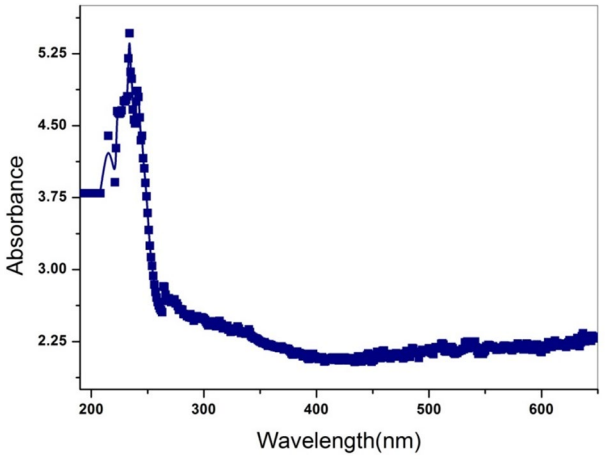

Fig. 4 Optical absorbance spectrum of BGCCD single crystal

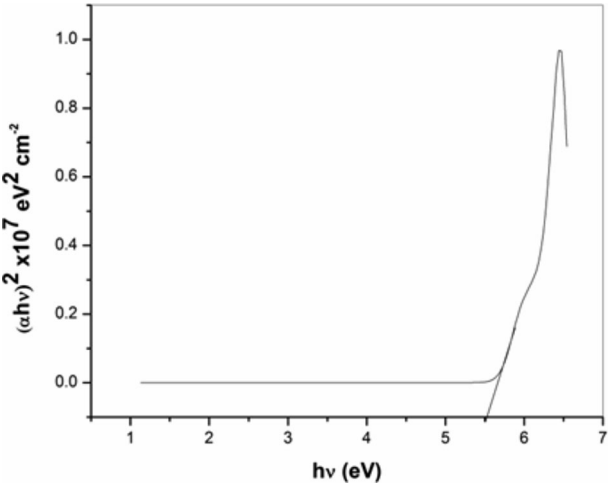

Fig. 5 Energy band gap of BGCCD single crystal

3.4 Microhardness studies

A study of microhardness in any system is very sensitive and has a direct association with the crystal structure. Device manufacturing relies heavily on microhardness characterization. Through the use of ZwickRoell micro-hardness tester, the mechanical property of the BGCCD crystal was determined. When subjected to 100 g, indentation causes the crystals typically smooth surface to start cracking as internal tensions are released locally (Tauc et al. 1974). Figure 6 shows the relationship among the hardness number (Hv) and the load (P). The possible qualitative explanation is that it is related to the indenter's penetration depth (Mott 1956). The indenter can only penetrate a limited number of surface layers when applied light stresses. The observed hardness is typical of these layers, and Hv grows with stress in this area; when stress rises, the whole impact is due to both the sample's outer and interior layers. The relationship between log d and log P is seen in Fig. 7. By using the least square fit approach to calculate the slope of the log P against log d plot, the value of the work

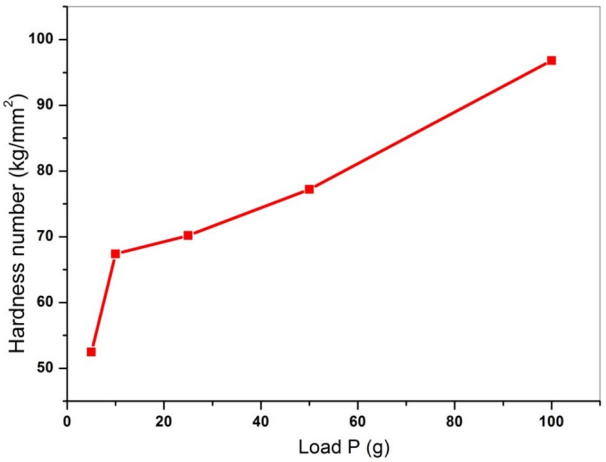

Fig. 6 Variation of hardness number through applied load for BGCCD single crystal

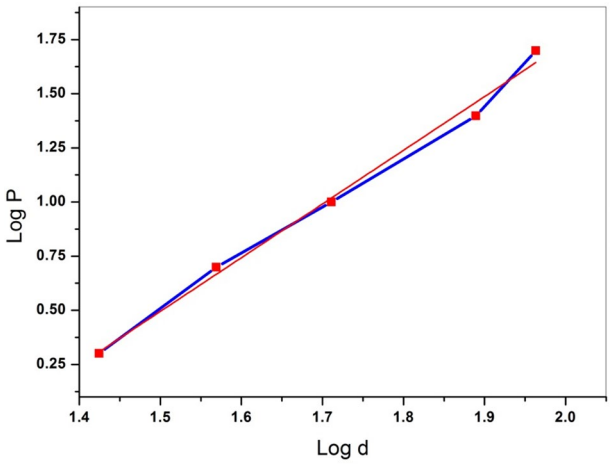

Fig. 7 Plot of log P Vs log d of BGCCD single crystal

hardening coefficient (Meyer 1908) n was establish to be 2.4. If the n values of a material are between 1 and 1.6, then that it is hard; otherwise, that it is soft, according to Onitsch (Onitsch 1947). Therefore, BGCCD crystal is a kind of soft material.

3.5 Dielectric studies

Applying varying temperatures to a single optical grade BGCCD crystal, the dielectric measurement studies were taken out utilizing the HIOKI 3520 LCR HI TESTER in the frequency range of 50 Hz to 2 MHz. A capacitor was created by applying silver paste on both sides of the crystal, which served as the dielectric medium. A parallel plate capacitor, consisting of the crystal sandwiched between two copper electrodes, was built. Various frequencies ranging from 50 Hz to 2 MHz were used to test the capacitance of the BGCCD. According to reference (Rao and Smakula 1996), the area (A) of the crystal, the permittivity of empty space (ε_0), and the capacitance (d) were used to calculate the dielectric constant.

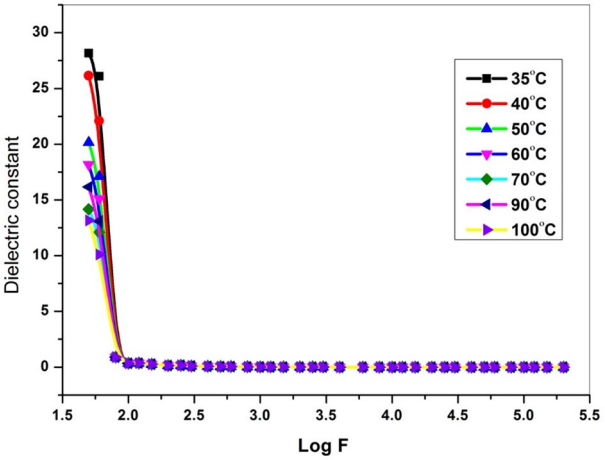

Fig. 8 Dielectric constant versus log frequency of BGCCD crystal

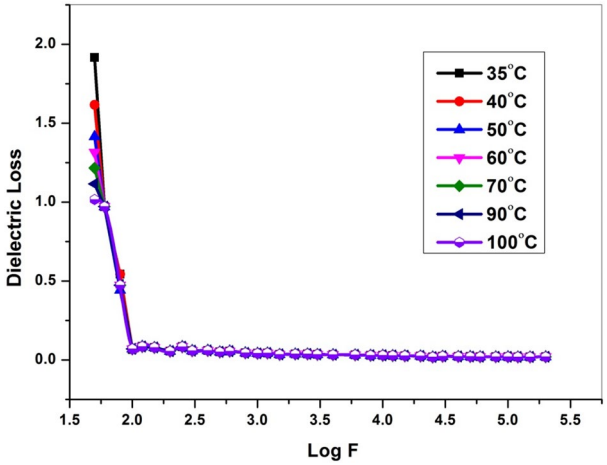

Fig. 9 Dielectric loss versus log frequency of BGCCD crystal

The dielectric constant's logarithmic fluctuation is seen in Fig. 8. Typically, the dielectric constant increases with decreasing frequency. Why the dielectric constant is so high at low frequencies and so low at high frequencies might be explained by the occurrence of all four polarizations: space charge, orientation, electronic, and ionic. The nett polarisation lowers at high frequencies, which causes the dielectric constant to fall since the space charge can't keep up with the alternating field (Deepthy and Bhat 2001). The values of the dielectric constant do not change much with regard to higher frequencies, as can be seen in Fig. 8. The dielectric constants also vary significantly over the temperature range. In order to get the dielectric loss, the dissipation factor (D) was substituted into the equation $\varepsilon'' = \varepsilon_i D$. Dielectric loss's logarithmic variation is seen in Fig. 9. Dielectric loss drops as frequency rises, as shown on the graph. Dielectric loss is frequency dependent; at low frequencies it is high and vice versa. The material's crystal has better optical quality with fewer defects, according to its low dielectric loss values (Sangwal 1987), which suggest it may be suitable for usage in NLO and electro-optic device applications.

3.6 Thermo-gravimetric and differential thermal analysis

In order to conduct thermo-gravimetric analysis (TGA) and differential thermal analysis (DTA) on the BGCCD sample, it was heated from ambient temperature to 800 °C and then maintained in a nitrogen atmosphere for 10 °C per minute. A Perkin Elmer STA 6000 thermal analyzer was used. Figure 10, which also displays the three primary phases of weight loss, reveals that the TGA/DTA spectrum to expose any weight loss when the temperature was maintained below 105 °C. Two water molecules and one glycine molecules are lost from the crystal lattice during the first step of weight loss is 33%, which happens between 121 °C and 184 °C. Within the temperature range of 185 °C to 383 °C, the second stage of weight loss is 22% takes place. At this point in weight reduction, it may have lost one glycine molecule. A cobalt and chloride molecules are being lost in the third stage of weight

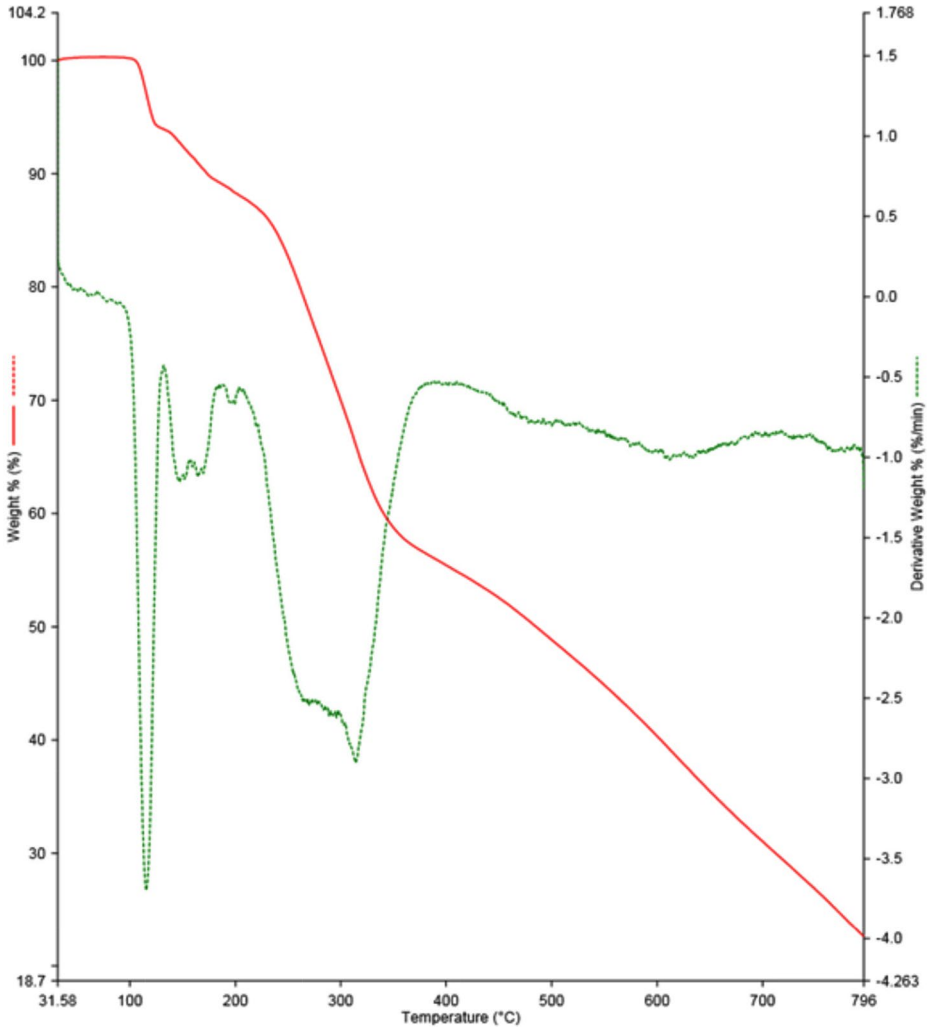

Fig. 10 TGA/DTA plot of grown BGCCD single crystal

loss happen among 384 °C and 800 °C, consequential in a total weight loss of 45%. It seems that the material starts to break down about 105 °C, according to the rate of weight loss. The endothermic peak seen at 110 °C on the DTA plot aligns well with the TGA result and represents the melting temperature of the BGCCD crystal. At these elevated temperatures, polymerisation opens the door to a wider variety of potential chemical reactions.

3.7 Etching analysis

The BGCCD crystal that was made was subjected to chemical etching tests using a polarised high-resolution optical microscope that has a motic camera. A variety of crystal defects, including growth triangle etch pits, surface grain boundaries, and microstructural faults, may be identified by the use of etching. The etchant was made using double-distilled water. Figure 11 (a) and Fig. 11 (b) show the etch patterns as pictures. The generated BGCCD single crystal is subjected to an etching study with varying etching times ranging from 5 to 10 s. Increasing the etching duration to 10 s causes an increasing number of uniform etch patterns to appear on the surface of the crystal. It may see growing indications and frequent etch pits upto the etching duration exceeding 10 s. While increasing etching duration the regular etch patterns as well increases.

3.8 Scanning electron microscopy with EDAX analysis

By analyzing the crystals using scanning electron microscopy (SEM), one may determine their surface form. The surface morphology of the generated crystal was examined using a scanning electron microscope (SEM) with a JSM 253 analyzer. Figure 12 (a) and 12 (b) show the micrographs of the BGCCD crystal that were acquired by scanning it at two different magnifications. Pictured in Fig. 12 (a) is the surface, which displays regular morphological behaviour of the atomic arrangement. Based in Fig. 12 (a), which shows a surface that is ideal for growth and contains small crystallites. As seen in Fig. 12 (b), the developed crystal displays a surface morphology resembling a hollow tube.

The energy dispersive X-ray analysis (EDAX) was used to analyze the elemental composition of the generated BGCCD single crystal. Using a JSM 253 SEM analyzer with Genesis

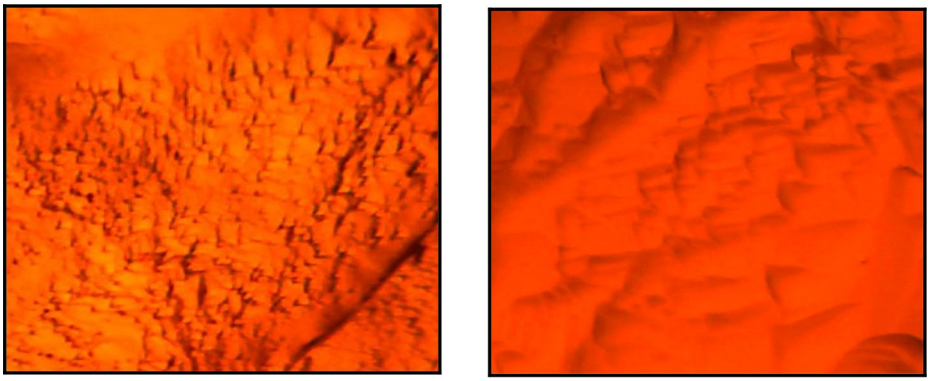

(a) 5 s (b) 10 s

Fig. 11 Etching patterns of BGCCD crystal for the etching time at (**a**) 5 s and (**b**) 10 s

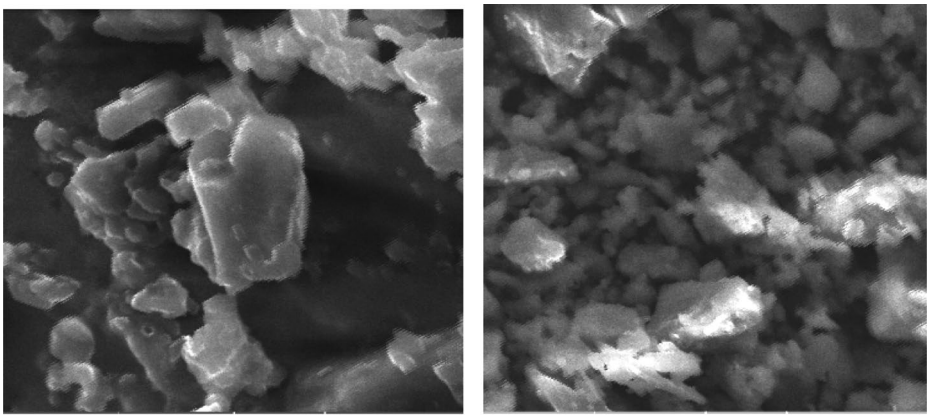

(a) 5 µm (b) 10 µm

Fig. 12 SEM micrograph of BGCCD crystal (**a**) 5 µm and (**b**) 10 µm

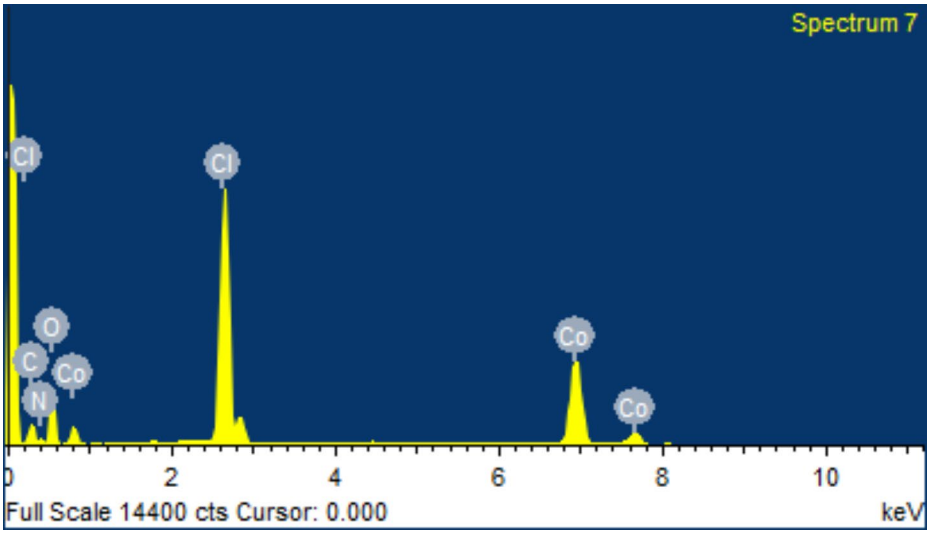

Fig. 13 EDAX spectrum of BGCCD grown single crystal

Eds software, the created BGCCD crystal was transmitted to EDAX to confirm the presence of nitrogen, carbon, oxygen, cobalt, and chloride ions. A single BGCCD crystal's EDAX spectrum is seen in Fig. 13. The proportion of different elements in the BGCCD single crystal is shown in Table 2.

3.9 Photoluminescence

The use of photoluminescence allows for the investigation of the crystal's flaws and faults without causing any damage. Using a Xenon flash lamp to excite the sample, the instru-

Table 2 Percentage of various elements present in the BGCCD single crystal

Element	Weight%	Atomic %
C	22.43	39.59
N	7.51	11.37
O	19.39	25.69
Cl	21.45	12.83
Co	29.22	10.51
Total	100	100

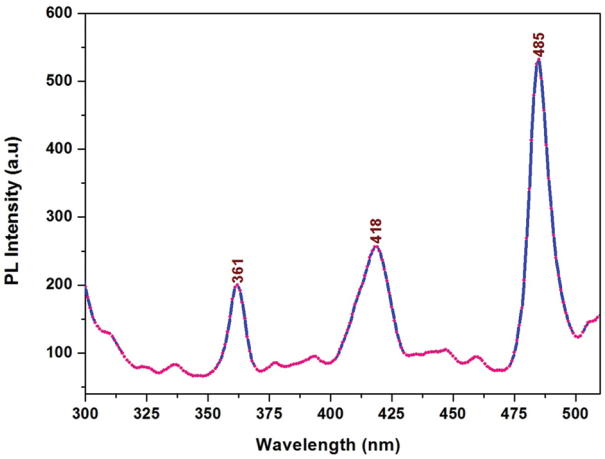

Fig. 14 PL excitation and emission spectrum of BGCCD single crystal

ment, a Cary Eclipse photoluminescence spectrometer, captured the photoluminescence (PL) emission spectra from 300 nm to 560 nm. The recorded emission spectra were stimulated at 361 nm, as seen in Fig. 14. The output signal was detected using a photomultiplier tube. The BGCCD emits a violet-blue light, as seen by its wide emission band with maxima at 418 nm and 485 nm. The electrons in the BGCCD crystal are able to make this transfer from donor to acceptor groups.

3.10 10 photoacoustic spectroscopy studies

Figure 15 shows the photoacoustic spectroscopy (PAS) block diagram, which was used to study the thermal diffusivity of the BGCCD crystal. A 250 W halogen lamp with modulated and collimated light is used to illuminate the specimen inside a hermetically sealed sample chamber. It is then set on a sample holder. When the surface of a sample comes into touch with radiation, it produces pressure waves. The temperature of the medium then fluctuates in response to these temperature gradients. In order to pick up on any changes, a microphone was placed within 1 mm of the sample. Afterwards, a sufficient frequency modulation was used to record the amplitude changes that resulted. Based on the square root of the chop-up frequency, Fig. 16 depicts the fluctuation of the photoacoustic (PA) signal for the BGCCD crystal. The graph illustrates that as the chop-up speed rises, the amplitude progressively drops and the PA signals' dependency (ω-1) is appealing and clearly proved.

Using the curve fitting approach, the BGCCD single crystal thermal diffusivity was estimated from Fig. 16 (Barros Melo and Faria 1995; Ishida and Rimdusit 1998). Table 3

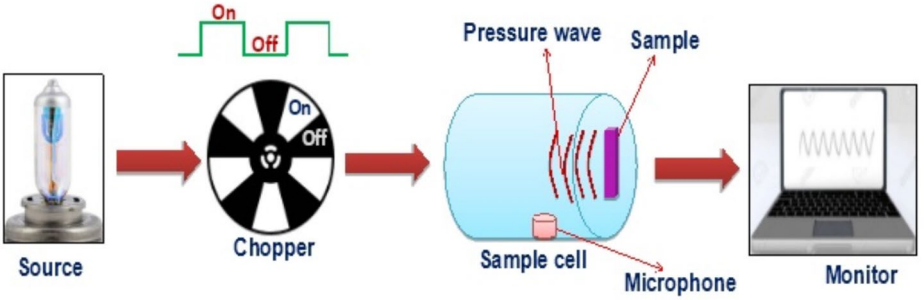

Fig. 15 Block diagram of PAS

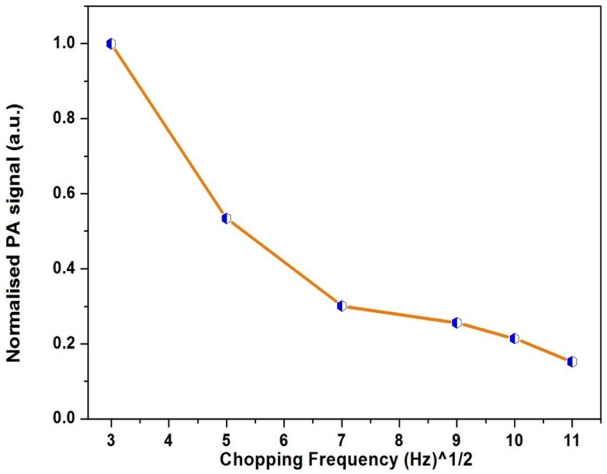

Fig. 16 Normalized PA signal for BGCCD single crystal vs. square root of chop-up frequency

Table 3 The BGCCD crystal's thermal diffusivity in relation to a few typical crystals

Materials	Thermal Diffusivity x 10^{-7} (m^2 / s)	Ref.
LTA	6.384	Jayapalan et al. (2018)
ADP	6.780	Sivakumar et al. (2019)
SA	20.442	Thirupathy et al. (2020)
NSH	8.398	Thirupathy et al. (2019)
CSPH	13.212	Preetha et al. (2023)
SSDH	7.985	Preetha et al. (2023)
BGCCD	13.974	[Present work]

reveals that the thermal diffusivity of BGCCD is 13.974×10^{-7} m^2/s, which was established by examining the data of numerous well-known NLO materials. The thermal diffusivity of the BGCCD crystal is bigger than that of an assortment of other notable NLO materials, including L-tartaric acid (LTA), Ammonium dihydrogen phosphate (ADP), Nickel sulphate

hexahydrate (NSH), Copper sulphate pentahydrate (CSPH), and Sodium sulfanilate dihydrate (SSDH). Many other kinds of devices, including as photonic, electrical, and opto-electronic ones, may benefit from the superior heat transport properties of BGCCD crystals.

4 Conclusion

Cobalt chloride bisglycine was produced through a method of slow evaporation. The grown crystal's SXRD analysis supported the predicted values of the unit cell parameters of BGCCD crystals, proving that the crystal displays a monoclinic structure. The FT-IR and FT Raman spectra of the generated crystals demonstrated the presence of chloride, cobalt, amino, and carboxyl groups. The produced crystal has a reduced cutoff wavelength of 288 nm, according to tests of optical absorbance. The produced crystals were classed as soft materials based on the Vickers microhardness value. Mechanical tests proved that reverse indentation has a size impact on generated crystals. The dielectric loss and dielectric constant of the created BGCCD crystal decrease with increasing frequency; these low values at high frequencies imply that the crystal is suited for NLO applications. The crystal that was created is thermally stable up to 120 °C, which makes it appropriate for electro-optical applications, as proven by TGA and DTA analysis. The etching study indicates that the etch pits develop in size when the etching time is extended from 5 s to 10 s. A scanning electron microscopy (SEM) analysis of the surface of the growing crystal revealed a structure that looked like a tube with holes in it. The elemental composition of the BGCCD single crystal may be determined by use EDAX. BGCCD emits a violet-blue light, as shown by the broad emission peaks at 418 nm and 485 nm in the PL analysis. The BGCCD crystal's superior thermal diffusivity compared to other famous NLO materials then it is suggested for photonic, electrical, and opto-electronic devices.

Acknowledgements The author T. Balakrishnan would like to acknowledge the Tamil Nadu State Council for Science and Technology (TNSCST), Tamil Nadu, India for providing financial support [Project ref. No. TNSCST/S & T Project/PS/RJ/2013–2014]. The authors gratefully acknowledge the scientific supports extended by Sophisticated Analytical Instrument Facility (SAIF), Indian Institute of Technology Madras, Chennai, 600036, India.

Author contributions P. Revathi: Conceptualization, formal analysis, Carrying out measurements, data curation, writing-original draft, writing review & editing; T. Balakrishnan: Conceptualization, supervision, formal analysis; J. Thirupathy: Conceptualization, investigation, writing review & editing. All authors have read and agreed to the published version of the manuscript.

Funding No funding was received.

Data availability No datasets were generated or analysed during the current study.

Declarations

Competing interests The authors declare no competing interests.

Conflict of interest The authors of this study would like to declare no conflict of interest.

Ethical approval The experiments carried out in this study did not involve human tissue.

References

Bagavan, N.V., Biochemistry, M.: Fourth ed., Academic, Harcourt, (2002)
Balakrishnan, T., Ramamurthi, K.: Cryst. Res. Technol. **41**, 1184–1188 (2006)
Balakrishnan, T., Ramamurthi, K.: Mater. Lett. **62**, 65–68 (2008)
Balakrishnan, T., Revathi, P., Krishnaveni, A., Thirupathy, J., Ramamurthi, K.: J. Mater. Sci: Mater. Electron. **29**, 16971–16982 (2018)
Balu, T., Rajasekaran, T.R., Murugakoothan, P.: Spectrochim Acta Part. A. **74**, 955–958 (2009)
Barros Melo, W.L., Faria, R.M.: Appl. Phys. Lett. **67**, 3892–3894 (1995)
Chemla, D.S., Zyss, J. (eds.): Nonlinear Optical Properties of Organic Molecules and Crystals. Academic, New York (1987)
Davis, E.A., Mott, N.F.: Philos. Mag. **22**, 903–922 (1970)
Deepthy, A., Bhat, H.L.: J. Cryst. Growth. **22**, 287–293 (2001)
Dhanaraj, P.V., Rajesh, N.P.: Phys. B. **406**, 12–18 (2011)
Eimerl, D., Velsko, S., Davis, L., Wang, F., Loiacono, G., Kennedy, G.: IEEE J. Quantum Electron. **25**, 179–193 (1989)
Fleck, M., Bohaty, L.: Acta Crystallogr. C. **60**, 291–295 (2004)
Gobinathan, L., Boopathy, K.: J. Adv. chem. **12**(11), 4523–4535 (2016)
Ishida, H., Rimdusit, S.: Thermochim Acta. **320**, 177–186 (1998)
Jayapalan, T., Sathiyadhas, S.J.D., Michael, J., Settu, B., Sathiyadhas Amalapushpam, M.B.D.: Cryst. Res. Technol. **53**, 1–5 (2018)
Khandpekar, M.M., Pati, S.P.: Opt. Commun. **284**, 818–823 (2011)
Lenin, M., Bhagavannarayana, G., Ramasamy, P.: Opt. Commun. **282**, 1202–1206 (2009)
Marder, S.R., Sohn, J.E., Stucky, G.D. (eds.): Materials for Nonlinear Optics. Am. Chem. Soc., Washington, DC (1991)
Matthias, B.T., Miller, C.E., Remeika, J.P.: Phys. Rev. **104**, 849–850 (1956)
Meyer, E.: Phys. Z. **66**, (1908)
Michel Fleck: Z. Kristallogr. **223**, 222–232 (2008)
Mott, B.W.: Microindentation Hardness Testing, Butterworth's, London, (1956)
Mott, N.F., Davis, E.A.: Electronic Processes in Non-Crystalline Materials. Clarendon, Oxford (1979)
Nakamoto, K.: Infrared and Raman Spectra of Inorganic and Coordination Compounds. Wiley, New York (1978)
NarayanaMoolya, B., Dharmaprakash, S.M.: J. Cryst. Growth. **293**, 86–92 (2006)
NarayanaMoolya, B., Dharmaprakash, S.M.: Mater. Lett. **61**, 3559–3562 (2007)
Narayanan, P., Venkataraman, S.: Z. Kristallogr. **142**, 52–81 (1975)
Neurath, H.: The Proteins, vol. 1. Academic (1972)
Onitsch, E.M.: Mikroskopie. **2**, 131 (1947)
Pepinsky, R., Vedam, K., Okaya, Y.: Phys. Rev. **110**, 1309–1311 (1958)
Preetha, N., Esakki Muthu, S., Thirupathy, J.: J. Mater. Sci: Mater. Electron. **34**, 932 (2023a)
Preetha, N., Oh, T.H., Esakki Muthu, S., Divya, S., Thirupathy, J.: Cryst. Res. Technol., 2300212 (2023b)
Ra. Shanmugavadivu, G., Ravi, A., Nixon Azariah: J. Phy Chem. Solids. **67**, 1858–1861 (2006)
Raju, B., Saritha, A., Jotani, M.M., Prasad, P.S.R., Hussain, K.A.: Phys. B. **407**, 188–192 (2012)
Rao, K.V., Smakula, A.: J. App Phys. **37**, 319–322 (1996)
Sangwal, K.: Etching of Crystals, North Holland Physics Publishing, Amsterdam, The Netherlands (1987)
Sankar, R., Ragahvan, C.M., Mohan Kumar, R., Jayavel, R.: J. Cryst. Growth. **309**, 30–36 (2007)
Sathiskumara, S., Balakrishnana, T., Ramamurthi, K.: Optik. **127**, 3410–3416 (2016)
Selvaraju, K., Valluvan, R., Kumararaman, S.: Mater. Lett. **60**, 2848–2850 (2006)
SenthilPandian, M., Ramasamy, P.: J. Cryst. Growth. **310**, 2563–2568 (2008)
Sivakumar, A., Suresh, S., Balachandar, S., Thirupathy, J.: Kalyana Sundar and S.A. Martin Britto Dhas. Opt. Laser Technol. **111**, 284–289 (2019)
Socrates, G.: Infrared and Raman Characteristic Group Frequencies. John Wiley, New York (2001)
Tauc, J., Amorphous, Semiconductors, L.: J. Plenum, New York, (1974)
Thirupathy, J., Sahaya Jude Dhas, S., Jose, M.: S Martin Britto Dhas Mater. Res. Express. **6**, 086206 (2019)
Thirupathy, J., Shaya Jude Dhas, S., Jose, M.: S Martin Britto Dhas J. Mater. Sci. Mater. Electron. **16**, 1–6 (2020)
Thomas Joseph Prakash, J., Vijayan, N., Kumararaman, S.: Spectrochim Acta Part. A. **71**, 1250–1252 (2008)
Venkataramanan, V., Subramanian, C.K., Bhat, H.L.: J. Appl. Phys. **77**, 6049–6051 (1995)
Versiane, O., Rodrigues, B.L., Ramos, J.M., Tellez, C.A., Felcman, J.: Spectrochim Acta Part. A. **65**, 1112–1119 (2006)